ANALYTICAL FRACTURE MECHANICS ANALYSIS OF THE PULL-OUT TEST INCLUDING THE EFFECTS OF FRICTION AND THERMAL STRESSES

John A. Nairn

Material Science & Engineering Department
University of Utah
Salt Lake City, UT 84112, USA

(Submitted 6/00, Revised 10/00)

ABSTRACT

The energy release rate for propagation of a debond in a single-fibre pull out test was derived analytically. The key finding was that an accurate analysis can be derived by a global energy analysis that includes effects of residual stresses and interfacial friction but does not need to include the details of the stress state at the interfacial crack tip. By comparison to finite elements analysis, it was verified that the analytical results are very accurate provided the debond tip is not too close to either end of the specimen. By casting the results in terms of net-specimen stress, it was possible to derive a general energy release rate result that applies to both the pull-out test and the related microbond test. The energy release rate expressions can be used to determine interfacial fracture toughness from single-fibre pull-out tests or microbond tests.

KEYWORDS: Pull-Out Test, Fracture Mechanics, Energy Release Rate, Debonding, Microbond Test, Residual Stresses, Friction.

1. INTRODUCTION

In a previous paper [1] the problem of a propagating fibre/matrix debond in a microbond specimen [2] was considered. Despite the complexity of the stresses around interface cracks, it was shown that the details of those crack tip stresses are normally not needed for deriving the energy release rate for debond propagation. The crack-tip stresses only matter when the debond tip is near either end of the specimen. For all other debond lengths, it is possible to derive an analytical expression for energy release rate by consideration only of boundary conditions, frictional stresses on the interface crack, and far-field mechanical and thermal stresses. The resulting energy release rate was verified by finite element analysis to be very accurate over almost the entire range of debond lengths. That energy release rate analysis was used to develop the microbond test into a fracture mechanics method for determining the mode II toughness of the fibre/matrix interface. It was found that both friction and residual stresses are important effects and must be included to determine the *true* interfacial fracture toughness [1].

A single-fibre test similar to the microbond test is the single-fibre, pull-out test [3]. In this paper, the methods of [1] were applied to the pull-out test. By using similar approximations, it was possible to derive an analytical expression for energy release rate for debond growth as a function of debond length including both the effects of interfacial friction and residual thermal stresses. Comparison to finite element analysis showed that this new result is very accurate except when the debond tip is near the point where the fibre enters the matrix or near the end of the embedded fibre length. The energy release rate expression can thus be used to deduce fracture toughness results from pull-out tests.

The analyses for the microbond test and the pull-out test are very similar, but there are two important differences. First, in the microbond test, the fibre is pulled while the top of the matrix is restrained. The force on the fibre is balanced by a restraining force on the matrix (see Fig. 1A). The net stress on the free droplet below the loading point is zero. In contrast, in the pull-out test the fibre is pulled while the matrix droplet is typically restrained on the opposite end (see Fig. 1B). This loading from both ends leads to a non-zero net stress throughout the specimen. By casting some terms in the analysis of this paper using net stress, it was possible to derive a general energy release rate expression that applies to both microbond and

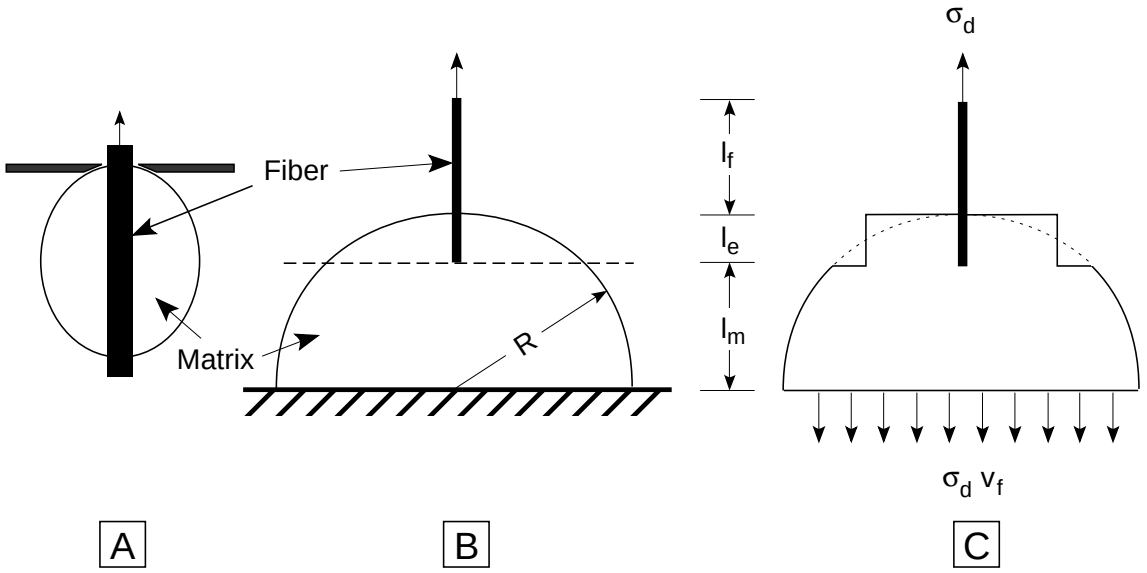

Fig. 1.: A. Microbond test geometry. B. Typical single-fibre, pull-out test with the fibre embedded in the top of a hemispherical droplet of radius R. l_f, l_e, and l_m are the lengths of free fibre, embedded fibre, and free matrix, respectively. C. The conversion of the embedded fibre zone to equivalent, concentric fibre and matrix cylinders. The radius of the matrix cylinder is chosen to match the total volume within the embedded fibre zone.

pull-out specimens. The net stress terms appear for the pull-out test, but are absent for the microbond test. Thus, the general expression derived here includes the results of [1] as a special case.

The second difference between microbond and pull-out tests is the amount of matrix material used. Microbond specimens typically use a small amount of matrix while pull-out tests use much more matrix. There are two terms in the final energy release rate analysis that depend on the rate of stress transfer between the matrix and the fibre. In the microbond test, these stress-transfer terms can be determined sufficiently accurately by shear-lag methods [1, 4]. In the pull-out test, the shear-lag methods have to be modified or replaced to get good stress-transfer results. The stress-transfer terms are only important when there is significant friction on the interface or when the total embedded fibre length is small. If friction is low and the embedded fibre length is long, the energy release rate in both the microbond test and in the pull-out test can be determined without need for any stress-transfer analysis.

2. THEORY

Figures 1 and 2 show a reduction of a real pull-out specimen to idealized coordinates. First, the restraint on the bottom of the matrix is replaced by a uniform traction that balances the traction applied to the top of the fibre. Second, the matrix region surrounding the embedded fibre is replaced by an *equivalent* cylinder of matrix. The radius of the matrix cylinder is chosen to preserve the total amount of matrix material within the zone of the embedded fibre (see Fig. 1). Finally, because the free fibre zone (of length l_f) and the free matrix zone (of length l_m) are under constant-traction, they release no energy as the debond propagates. The energy release rate analysis can thus focus on the concentric cylinder model in Fig. 2. The fibre is loaded by a stress of σ_d while the opposite end of the specimen is loaded by a uniform stress of $v_f\sigma_d$ where v_f is the fibre volume fraction in the equivalent cylinder model of the embedded fibre zone. The stress σ_e shown on the bottom of the fibre is the actual internal stress on the end of the embedded fibre.

Using the general composite fracture mechanics methods from [5] and applying them to the geometry in Fig. 2 using the methods of [1], the exact energy release rate for debond growth can be written as

$$G(a) = \frac{r_f}{4}\left\{\sigma_d\frac{d}{da}\big(\langle w_f(a)\rangle - \langle w(a-l_e)\rangle\big) - k\frac{d}{da}\int_0^a \big(\langle w_f(z)\rangle - \langle w_m(z)\rangle\big)dz\right.$$

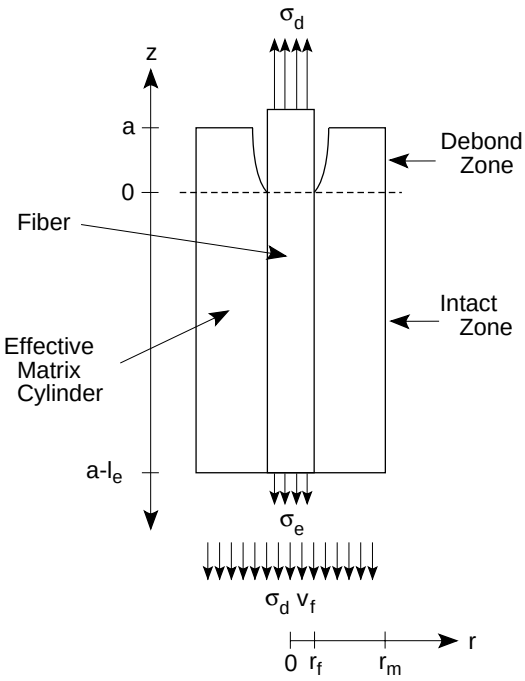

Fig. 2.: An equivalent, concentric-cylinder model for the embedded fibre zone of a single-fibre pull-out specimen. The origin of the z axis is placed at the debond tip. The net stress of $\sigma_0 = v_f \sigma_d$ is applied to the bottom of the specimen as a uniform traction. The actual stress on the end of the embedded fibre internal to the specimen is designated by σ_e.

$$+ l_e \Delta T \left[(\alpha_A - \alpha_m) \frac{d\overline{\sigma_{zz}^{(f)}}}{da} + \alpha_T \frac{d}{da} \left(\overline{\sigma_{rr}^{(f)}} + \overline{\sigma_{\theta\theta}^{(f)}} \right) + \frac{v_m}{v_f} \alpha_m \frac{d}{da} \left(\overline{\sigma_{rr}^{(m)}} + \overline{\sigma_{\theta\theta}^{(m)}} \right) \right] \Bigg\} \qquad (1)$$

Here the z-axis origin has been placed at the tip of the debond (see Fig. 2), a is the length of the debond, r_f is the fibre radius, $\langle w_f(a) \rangle$ is the average axial fibre displacement on the top of the specimen, $\langle w(a - l_e) \rangle$ is the average axial displacement at the bottom of the specimen, $k = 2\tau_f / r_f$ is a friction term related to the absolute value of the interfacial friction stress (τ_f), $\langle w_f(z) \rangle$ and $\langle w_m(z) \rangle$ are the average fibre and matrix axial displacements as a function of position within the debond zone, l_e is the embedded fibre length, ΔT is the difference between the specimen temperature and the stress-free temperature, α_A and α_T are the axial and transverse thermal expansion coefficients of the fibre (which is assumed to be transversely isotropic), α_m is the thermal expansion coefficient of the matrix (which is assumed to be isotropic), v_f and v_m are the volume fractions of the fibre and matrix in the equivalent cylinders, and $\overline{\sigma_{jj}^{(i)}}$ are phase-averaged stresses in the fibre or matrix [1, 5].

There are two changes between (1) and the corresponding result for the microbond test [1]. First, the term involving $\langle w(a - l_e) \rangle$ arises from the tractions at the *bottom* of the specimen; the corresponding term in the microbond analysis involves the matrix displacement at the *top* of the specimen. Second, the friction term arises from frictional work on the interface. The term here has already been simplified using approximations introduced later in [1]. The two approximations are to assume that the magnitude of the friction stress, τ_f, is constant over the entire interface and to assume that the amount of sliding at the interface can be approximated by the difference in *average* axial displacements in the fibre and the matrix. Although we use the term "friction" for the interfacial shear stress, the use of a constant τ_f over the debond zone is not modeling Coulomb friction. We used a constant friction stresses as an approximation to friction in order to get an analytical result. A rigorous representation of Coulomb friction requires numerical calculations [6]. Furthermore, there is evidence that interfacial shear stress on debonds in pull-out tests may not arise from

Coulomb friction. In linear-elastic Coulomb friction, the friction stress should be proportional to the radial stress which must be proportional to the axial load. Raman experiments on pull-out specimens, however, show that the shear stress in the debond zone is not proportional to applied load and is often roughly constant [7]. A constant interfacial shear stress is thus used here as an approximate model for frictional loading and as a tool to account for other sources of interfacial shear stress that may not be due to Coulomb friction.

Within the debond zone ($0 < z < a$), the *average* axial and transverse stresses in the fibre and matrix can be written as

$$\begin{aligned} \left\langle \sigma_{zz}^{(f)}(r,z) \right\rangle &= \sigma_d + k(z-a) \qquad \text{and} \qquad \left\langle \sigma_{zz}^{(m)}(r,z) \right\rangle = -\frac{v_f k(z-a)}{v_m} \\ \left\langle \sigma_{rr}^{(f)}(z) + \sigma_{\theta\theta}^{(f)}(z) \right\rangle &= 0 \qquad \text{and} \qquad \left\langle \sigma_{rr}^{(m)}(z) + \sigma_{\theta\theta}^{(m)}(z) \right\rangle = 0 \end{aligned} \tag{2}$$

The average axial stress in the fibre consists of the applied stress, σ_d, reduced by stress transfer to the matrix through friction at the interface (see [1] but note that that paper has a misprint in the sign of the k term. Despite that misprint, the remaining equations in that paper are correct). The fibre stress decreases from σ_d where the fibre enters the matrix ($z = a$) to $\sigma_d - ka$ at the debond tip ($z = 0$). This analysis assumes that friction is low enough that only partial stress transfer occurs in the debond zone. In other words, this analysis requires $ka < \sigma_d$. The average axial matrix stress is determined by force balance. Notice that the net axial stress is

$$\sigma_0 = v_f \left\langle \sigma_{zz}^{(f)}(r,z) \right\rangle + v_m \left\langle \sigma_{zz}^{(m)}(r,z) \right\rangle = v_f \sigma_d \tag{3}$$

In contrast, $\sigma_0 = 0$ in the microbond analysis. The radial and hoop stresses are complicated, especially near the debond tip. As long as the debond tip is not too close to either end, however, the complicated radial and hoop stresses can be expected to remain constant in magnitude but to propagate along with the crack. When evaluating energy release rate by taking derivatives as a function of debond length, such constant stresses will drop out. Thus it assumed that the average transverse stresses in the debond zone are zero.

Within the intact zone ($a - l_e < z < 0$), the *average* axial and transverse stresses in the fibre and matrix can be written as [1]

$$\begin{aligned} \left\langle \sigma_{zz}^{(f)}(z) \right\rangle &= \psi_\infty + (\sigma_e - \psi_\infty)F(z-a+l) + (\sigma_d - k\,a - \psi_\infty)F(-z) \\ \left\langle \sigma_{rr}^{(f)}(z) + \sigma_{\theta\theta}^{(f)}(z) \right\rangle &= 2\sigma_\infty \\ \left\langle \sigma_{zz}^{(m)}(z) \right\rangle &= \frac{v_f \left(\sigma_d - \left\langle \sigma_{zz}^{(f)}(z) \right\rangle \right)}{v_m} \\ \left\langle \sigma_{rr}^{(m)}(z) + \sigma_{\theta\theta}^{(m)}(z) \right\rangle &= -\frac{2v_f \sigma_\infty}{v_m} \end{aligned} \tag{4}$$

Here ψ_∞ and σ_∞ are the axial fibre stress and interfacial radial stress for infinitely long concentric cylinders subjected to net axial stress $\sigma_0 = v_f\sigma_d$ and temperature differential ΔT. The function $F(z)$ is the solution to an underlying stress-transfer problem; it is the average axial fibre stress in concentric cylinders subjected to unit normal stress on the fibre and a balancing $-v_f/v_m$ stress on the matrix, both at $z = 0$. Analogous to the analysis in the debond zone, it was assumed that any complicated radial and hoop stresses associated with the debond tip drop out when evaluating energy release rate. The remaining average transverse stresses are those associated with far-field transverse stresses in a concentric cylinder model [1]. The average axial stress in the fibre is the superposition of three problems - far-field fibre stress plus $(\sigma_e - \psi_\infty)$ at the bottom of the fibre plus $(\sigma_d - k\,a - \psi_\infty)$ at the debond tip. The axial stresses are identical to the results in [1] except for the new σ_e term and the addition of the $v_f\sigma_d$ net stress term to the matrix axial stress.

Evaluation of energy release rate using (1) requires evaluation of phase average stresses and average axial displacements. The required phase-averaged stresses in terms of average stresses can be evaluated using the above results and

$$\overline{\sigma_{ij}^{(m \text{ or } f)}} = \frac{1}{l_e} \int_{-(l_e-a)}^{a} \left\langle \sigma_{ij}^{(m \text{ or } f)} \right\rangle dz \tag{5}$$

The required average axial displacements can be evaluated by integrating the axial strains:

$$\langle w_f(z) \rangle = \int_0^z \left\langle \varepsilon_{zz}^{(f)}(u) \right\rangle du \qquad \text{and} \qquad \langle w_m(z) \rangle = \int_0^z \left\langle \varepsilon_{zz}^{(m)}(u) \right\rangle du \tag{6}$$

The average strains can be found from

$$\begin{aligned} \left\langle \varepsilon_{zz}^{(f)}(u) \right\rangle &= \frac{\left\langle \sigma_{zz}^{(f)}(u) \right\rangle}{E_A} - \frac{\nu_A \left\langle \sigma_{rr}^{(f)}(u) + \sigma_{\theta\theta}^{(f)}(u) \right\rangle}{E_A} + \alpha_A \Delta T \\ \left\langle \varepsilon_{zz}^{(m)}(u) \right\rangle &= \frac{\left\langle \sigma_{zz}^{(m)}(u) \right\rangle}{E_m} - \frac{\nu_m \left\langle \sigma_{rr}^{(m)}(u) + \sigma_{\theta\theta}^{(m)}(u) \right\rangle}{E_m} + \alpha_m \Delta T \end{aligned} \tag{7}$$

where E_A is the axial modulus of the fibre and E_m is the modulus of the matrix. The specimen displacement at the bottom is found by averaging the fibre and matrix displacements:

$$\langle w(a - l_e) \rangle = v_f \langle w_f(a - l_e) \rangle + v_m \langle w_m(a - l_e) \rangle \tag{8}$$

Finally, by an exact elasticity analysis for two infinitely-long concentric cylinders, the far field stress terms can be written as

$$\psi_\infty = -\frac{C_{13}\sigma_0}{C_{33}} - \frac{D_3 \Delta T}{C_{33}} \qquad \text{and} \qquad \sigma_\infty = \frac{v_m \sigma_d}{A_0} \left(\frac{C_{13} A_3}{C_{33}} - \frac{\nu_m}{v_m E_m} \right) + \frac{v_m \Delta T}{v_f A_0} \left(\frac{A_3 D_3}{C_{33}} - (\alpha_T - \alpha_m) \right) \tag{9}$$

where the constants A_i, D_3, and C_{ij} depend only on fibre and matrix properties and are defined in the *Appendix* [8].

The above results can be substituted into (1) leading to a closed-form expression for energy release rate for debond growth as a function of specimen geometry and loading terms σ_d, ΔT, and k. The resulting expression (which is not given here) is very complex, but many terms are typically negligible in polymer-matrix composites. The key next step is rewrite the results in terms of the effective axial modulus, E_c, and effective thermal expansion coefficient, α_c, of an infinitely-long concentric fibre/matrix cylinder model. Writing the far-field, fibre axial strain in terms of effective properties gives

$$\frac{v_f \sigma_d}{E_c} + \alpha_c \Delta T = \frac{\psi_\infty}{E_A} - \frac{2\nu_A \sigma_\infty}{E_A} + \alpha_A \Delta T \tag{10}$$

Substituting the results for ψ_∞ and σ_∞ in (9) into (10) and equating the mechanical and thermal parts leads to exact elasticity results for E_c and α_c which can be written as

$$\begin{aligned} E_c &= v_f E_A + v_m E_m + E_c^* \\ \alpha_c &= \frac{\alpha_A v_f E_A + \alpha_m v_m E_m}{E_c} + \alpha_c^* \end{aligned} \tag{11}$$

The first terms in these results are the simple rule-of-mixtures results for axial modulus and axial thermal expansion. The second terms are extra terms that arise in the exact analysis of concentric cylinder models [9, 10]. They are exactly zero when the Poisson ratio of the fibre and the matrix are equal ($\nu_A = \nu_m$). For typical polymer-matrix composites, they are much smaller than the rule-of-mixtures terms and therefore can be neglected.

Rewriting the complex expression for $G(a)$ mentioned above in terms of E_c and α_c, substituting the results in (11), and ignoring all terms involving E_c^* and α_c^*, the energy release rate for debond growth in the single-fibre, pull-out test can be written as:

$$\begin{aligned} G(a) &= \frac{r_f}{2} \Bigg\{ C_{33s} \bar{\sigma}^2 + 2 D_{3s} \bar{\sigma} \Delta T + \left(\frac{D_3^2}{C_{33}} + \frac{v_m (\alpha_T - \alpha_m)^2}{v_f A_0} \right) \Delta T^2 \\ &\quad - \left[\frac{\sigma_0}{2} \left(\frac{1}{E_A} - \frac{1}{E_m} \right) + D_{3s} \Delta T \right] \left[k\, C_T(a) - \left(\bar{\sigma} + \frac{2 D_3 \Delta T}{C_{33}} + \sigma_e - \frac{\sigma_0}{2 C_{33s} v_m E_m} \right) C_T'(a) \right] \Bigg\} \end{aligned} \tag{12}$$

where $\bar{\sigma}$ is a reduced debonding stress which is defined by

$$\bar{\sigma} = \sigma_d - k\, a - \frac{\sigma_0 E_A}{v_f E_A + v_m E_m} \tag{13}$$

and $C_T(a)$ is a cumulative stress-transfer function defined by:

$$C_T(a) = \int_0^{l_e-a} F(z)\,dz \tag{14}$$

The remaining constants, A_i, D_i, and C_{ij}, are defined in the *Appendix*. Equation 12 has been written with terms involving the net specimen stress, $\sigma_0 = v_f\sigma_d$, and the stress at the end of the embedded fibre, σ_e. For the microbond test, both these stresses are zero. Thus, (12) reduces exactly to the microbond result in [1] by setting $\sigma_0 = \sigma_e = 0$. Finally, the result can be simplified further by making one additional assumption about the stress at the end of the embedded fibre, σ_e. Here we assume that the fibre stress in the pull-out test reaches the far-field fibre stress or ψ_∞. Furthermore, using the approximation that $E_c^* = \alpha_c^* = 0$, ψ_∞ can be rewritten as

$$\sigma_e = \psi_\infty \approx \frac{\sigma_0}{2C_{33s}v_mE_m} - \frac{D_3\Delta T}{C_{33}} \tag{15}$$

In contrast, for the microbond test, the end of the fibre is unloaded and thus $\sigma_e = 0$. Substituting both σ_e assumptions into (12) the energy release rate for debond growth in both the pull-out test and the microbond test can be written as

$$\begin{aligned} G(a) \;=\; & \frac{r_f}{2}\Bigg\{C_{33s}\bar\sigma^2 + 2D_{3s}\bar\sigma\Delta T + \left(\frac{D_3^2}{C_{33}} + \frac{v_m(\alpha_T-\alpha_m)^2}{v_fA_0}\right)\Delta T^2 \\ & - \left[\frac{\sigma_0}{2}\left(\frac{1}{E_A}-\frac{1}{E_m}\right) + D_{3s}\Delta T\right]\left[k\,C_T(a) - \left(\bar\sigma + \frac{(1+m)D_3\Delta T}{C_{33}}\right)C_T'(a)\right]\Bigg\} \end{aligned} \tag{16}$$

where m is a flag that is $m = 0$ for the pull-out test but $m = 1$ for the microbond test. In many cases, it is found that $D_3 \approx D_{3s}$ and $C_{33} \approx C_{33s}$, but some sample calculations showed differences of over 10% are possible. There is little incentive to introduce these extra approximations because it is already easy to make calculations using (16).

Two interesting limits of (16) are when the embedded fibre length is long and when the interface is frictionless. For long embedded fibres, the function $F(z)$ will decay from $F(z) = 1$ at $z = 0$ to $F(z) = 0$ long before the end of the bonded interface zone at $z = l_e - a$. Clearly, this limit implies $C_T(a)$ is a constant which further implies that $C_T'(a) = 0$. Writing the constant as $C_T(a) = 1/\beta$ (for reasons that become apparent below), the long-fibre limiting result is

$$\begin{aligned} G_\infty(a) = \lim_{l_e\to\infty} G(a) \;=\; & \frac{r_f}{2}\Bigg\{C_{33s}\bar\sigma^2 + 2D_{3s}\bar\sigma\Delta T + \left(\frac{D_3^2}{C_{33}} + \frac{v_m(\alpha_T-\alpha_m)^2}{v_fA_0}\right)\Delta T^2 \\ & - \frac{k}{\beta}\left[\frac{\sigma_0}{2}\left(\frac{1}{E_A}-\frac{1}{E_m}\right) + D_{3s}\Delta T\right]\Bigg\} \end{aligned} \tag{17}$$

This result reduces to the long-fibre limit in [1] for the microbond test which has $\sigma_0 = 0$ and $m = 1$ (but note that there is sign error in the k/β term in the long-fibre limit in [1] even though the full equation for $G(a)$ in that paper is correct). The frictionless limit for any fibre length or for long fibre lengths can easily be found by setting $k = 0$ in (16) or (17), respectively. Note that for frictionless interfaces and long fibres that all terms involving $C_T(a)$ and $C_T'(a)$ drop out. In other words, for this special case, $G_\infty(a)$ can be determined without the need for any stress analysis to find $C_T(a)$.

3. RESULTS

The accuracy of (16) can be checked by comparison to finite element calculations. To get explicit results, however, a result for the stress-transfer function $C_T(a)$ is needed. In real experiments, $C_T(a)$ could be determined by experiments such as by Raman spectroscopy [7]. For comparison to linear-elastic, finite element calculations, it is better to determine $C_T(a)$ by elasticity analysis of the pull-out test. Here it was found that as long as v_f is not too low, that $C_T(a)$ can be found with sufficient accuracy by a shear-lag

analysis. From [1], the relevant results are:

$$C_T(a) = \frac{1}{\beta}\left[\coth\beta(l_e-a) - \operatorname{csch}\beta(l_e-a)\right] \tag{18}$$

$$C_T'(a) = -\frac{1}{2}\operatorname{sech}^2\left(\frac{\beta(l_e-a)}{2}\right) \tag{19}$$

where β is the shear-lag parameter defined by [4, 11, 12]

$$\beta^2 = \frac{2}{r_f^2 E_A E_m}\left[\frac{E_A v_f + E_m v_m}{\frac{v_m}{4G_A} + \frac{1}{2G_m}\left(\frac{1}{v_m}\ln\frac{1}{v_f} - 1 - \frac{v_f}{2}\right)}\right] \tag{20}$$

where G_A and G_m are the axial shear-modulus of the fibre and the shear modulus of the matrix. Note that this shear-lag parameter is different than the Cox parameter [13] commonly quoted in the literature. The Cox parameter is incorrect while the parameter in (20), originally derived by Nayfeh [12], has been shown to give good results provided the fibre volume fraction is not too low [4]. In the long-fibre limit, $C_T(a) \to 1/\beta$ and $C_T'(a) \to 0$; thus an alternate view of the shear-lag parameter is that it is analogous to the inverse of the cumulative stress transfer function defined here. In the previous section, $G_\infty(a)$ was written in terms of β. In a shear-lag analysis, this β is the shear-lag parameter. Equation 17, however, is not a shear-lag result. Any alternate stress-analysis can be used to find the constant $C_T(a)$ which can then be set equal to $1/\beta$ and substituted into (17) to get a long-fibre, limiting result for that stress-analysis method.

Figure 3 gives a comparison between the analytical results and finite element analysis. In brief, the comparison was for glass fibres ($E_A = E_T = 73{,}000$ MPA, $\nu_A = \nu_T = 0.17$, $\alpha_A = \alpha_T = 5$ ppm/°C, $G_A = 31{,}197$ MPa) embedded in a polymer matrix ($E_m = 3300$ MPa, $\nu_m = 0.34$, $\alpha_m = 48$ ppm/°C, $G_m = 1231$ MPa). The fibre radius was $r_f = 10.5$ μm, had an embedded length of 420 μm, and specimen volume fraction of $v_f = 1\%$. The specimen was loaded with $\sigma_d = 400$ MPa, thermal load $\Delta T = -100$°C, and interfacial friction of $\tau_f = 1$ MPa. The finite element analysis used axisymmetric, 8-noded, isoparametric elements. The energy release rate as a function of debond length was found by a modified crack closure technique [15]. The analytical results are for the full analysis in (16) and for the long-fibre limit in (17). The equations in this paper give the total energy release rate; the finite element results show that the total energy release rate is essentially a pure mode II energy release rate. The full analysis and the finite element analysis agree extremely well provided the debond length is neither too long nor too short. Many approximations used here relied on the debond tip not being too close to either end. The results in Fig. 3 show that when that condition holds the analytical result is very accurate. When the debond tip is near either end, the finite element analysis and the analytical result disagree. It is not certain, however, that the finite element results should be viewed as correct in these extremes. The finite element analysis has is own set of problems when the debond tips get too close to boundaries, The analytical solution, which is smoother, may even provide a better representation of the energy release rate as a function of debond length than the finite element analysis. This issue could be resolved by more refined finite element analysis.

The long-fibre limit agrees well with the full analysis and with finite element analysis only for the shorter debond lengths. As the debond length increases, the term $l_e - a$ gets smaller and the long-fibre limit becomes increasingly less accurate. From (18), it is apparent that the long-fibre limit requires

$$l_e - a >> \frac{1}{\beta} \tag{21}$$

For these sample calculations, $1/\beta = 28.3$ μm. The long-fibre limit in Fig. 3 is only accurate when $l_e - a >$ 300 μm or when $l_e - a$ is about an order of magnitude larger than β.

4. EXPERIMENTAL CONSIDERATIONS

The volume fractions used in A_i, D_i, and C_{ij} refer to the equivalent fibre volume fraction within the zone containing the embedded fibre. A common specimen geometry in single-fibre pull out tests is to place a large, hemispherical droplet on a surface and embed the fibre into the top of the hemisphere [16] (see Fig. 1). By equating the volume of the specimen above the bottom of the embedded fibre (the zone above the dotted

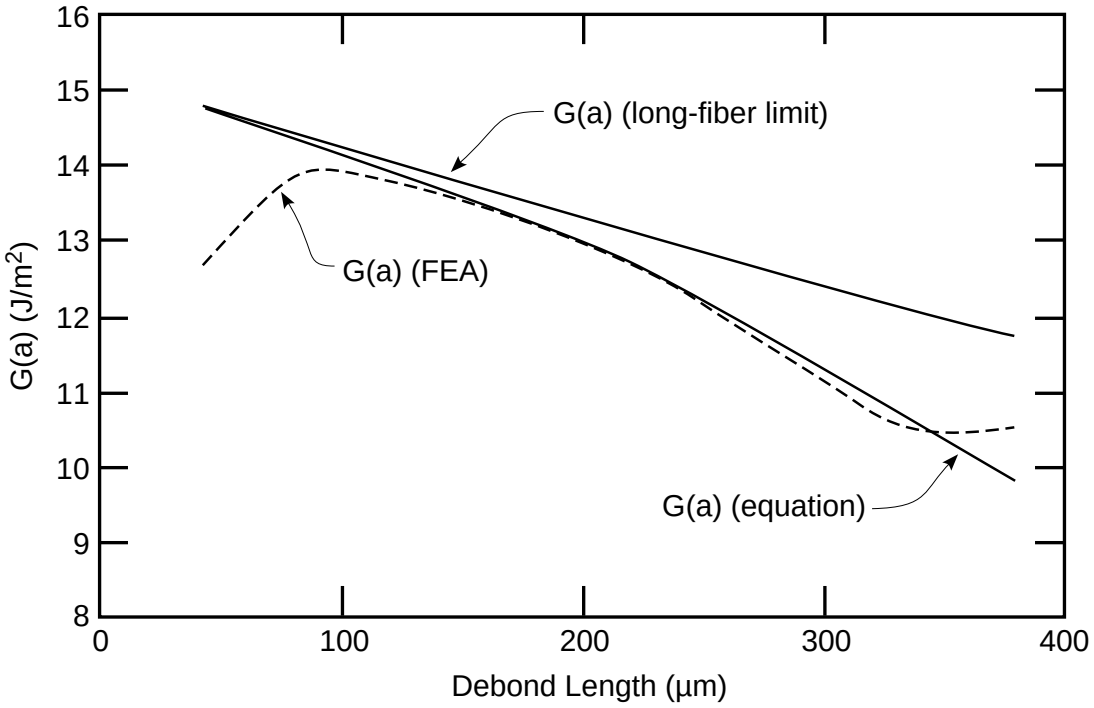

Fig. 3.: A sample calculation of $G(a)$ for a single-fibre pull out test of a glass fibre in a polymeric matrix with the fibre volume fraction of $v_f = 1\%$. The "equation" results were calculated from (16); the "long-fibre limit" results were calculated from (17); the dashed line is the result of finite element calculations.

line in Fig. 1) to the volume of the equivalent cylinder, the effective matrix outer radius can be calculated from:

$$r_m = \sqrt{l_e\left(R - \frac{l_e}{3}\right)} \tag{22}$$

The effective fibre volume fraction is $v_f = r_f^2/r_m^2$. In typical pull-out tests, $R >> r_f$, l_e and the effective fibre volume fractions are very low — typically $v_f \sim 0.03\%$ [17]. For volume fractions that low, all constants can be evaluated with 2% accuracy simply by using $v_f = 0$ which dispenses of the need for estimating an effective fibre volume fraction. The insensitivity of the constants to volume fraction at low fibre volume fraction suggests the analysis will be insensitive to the details of the matrix boundary. In other words, the effective cylinder analysis is probably adequate.

Although A_i, D_i, and C_{ij} can be stably evaluated for any fibre volume fraction, the same situation does not hold for the shear-lag parameter β, which is one method of finding $C_T(a)$. The shear-lag β approaches zero as v_f approaches zero. In other words, shear-lag analysis breaks down when the fibre volume fraction is too low. Some comparisons between shear-lag analysis and finite element analysis for high-modulus fibres in a polymeric matrix suggest that shear-lag analysis works for fibre volume fractions down to about $v_f = 1\%$, or maybe slightly lower for very stiff fibres or very compliant matrices [4]. If shear-lag analysis is used to find $C_T(a)$ at lower v_f, the only option is to calculate β using yet another effective fibre-volume fraction that characterizes stress transfer into the fibre. This new v_f can be determined by other elasticity analyses or by experiments [4]. Note that this new effective fibre volume fraction for shear-lag analysis of stress transfer should *only* be used for finding β; the fibre volume fraction used for evaluating A_i, D_i, and C_{ij} should be derived from the actual specimen as described above. Furthermore, if $C_T(a)$ is evaluated by a non-shear-lag method that works at all volume fractions, than it can derived from actual specimen dimensions as well, eliminating the need for the shear-lag β. For example, if $C_T(a)$ is *measured* using Raman experiments [7], it can be directly determined without β by evaluation of the average fibre stress in the intact zone (see Fig. 2).

The only complication is that Raman experiments measure actual fibre stress while $C_T(a)$ is defined from a normalized stress analysis. From the average stresses in the intact zone in (4), it is easy to show that $C_T(a)$ can be calculated from Raman experiments using

$$C_T(a) = (l_e - a)\left(\frac{\left\langle \sigma^{(f)}_{zz,intact}\right\rangle - \psi_\infty}{\sigma_1 - \psi_\infty + \sigma_2 - \psi_\infty}\right) \tag{23}$$

where $\left\langle \sigma^{(f)}_{zz,intact}\right\rangle$ is the average axial fibre stress measured in the intact zone, and σ_1 and σ_2 are the measured axial fibre stress at the beginning and the end of the intact zone. The far-field stress ψ_∞ could be measured far from any fibre end or calculated using (9) or perhaps sufficiently accurately by (15).

To evaluate interfacial fracture toughness from experimental pull-out results, one substitutes those results into (16). The required experimental results are failure stress (σ_d), the thermal stress term (ΔT), interfacial friction (τ_f), embedded fibre length (l_e), fibre radius (r_f), effective matrix radius (r_m from (22) and hemisphere radius R or some other method for other specimen geometries), debond length (a), and, if shear-lag analysis is used, an effective fibre volume fraction solely for calculation of β. Most of these parameters are readily available for pull-out results, but two require special mention. First is the debond length. The energy release rate is a function of debond length and becomes a strong function of debond length when there is interfacial friction. Thus, to derive the correct toughness requires knowledge of both debond load and initial debond length. The best results require observations of debond length during the experiments. A possible alternative is to record just the initiation of debonding and calculate toughness using $a = 0$. In typical pull-out tests, however, initiation of debonding occurs well below the peak load [18]. In other words, data that only records peak force can not be analyzed unless debond length at that load was also recorded.

Second is interfacial friction. The energy release rate depends on the amount of interfacial friction. Friction becomes more important as the debond gets longer, but it even influences the toughness for zero debond length. The *true* interfacial toughness can only be determined if some method is used to determine the actual amount of friction on the debonded interface. If friction is ignored, the toughness calculated by (16) will be too large. All calculations from experimental results can easily be done in spread sheet software. A Microsoft Excel spread sheet for such calculations can be downloaded from the Internet [19] or obtained from the author.

ACKNOWLEDGEMENTS

This work was supported by a grant from the Mechanics of Materials program at the National Science Foundation (CMS-9713356). The author thanks Serge Zhandarov for his pull-out work that lead to the need for this new analysis and for his comments.

APPENDIX

The defined A_i, C_{ij}, and D_i required for the calculations described in this paper are listed below:

$$v_f A_0 = \frac{v_m(1-\nu_T)}{E_T} + \frac{v_f(1-\nu_m)}{E_m} + \frac{1+\nu_m}{E_m} \tag{24}$$

$$A_3 = -\left(\frac{\nu_A}{E_A} + \frac{v_f\nu_m}{v_m E_m}\right) \tag{25}$$

$$C_{33s} = \frac{1}{2}\left(\frac{1}{E_A} + \frac{v_f}{v_m E_m}\right) \tag{26}$$

$$C_{33} = C_{33s} - \frac{v_m A_3^2}{v_f A_0} \tag{27}$$

$$C_{13} = -\frac{1}{2v_m E_m} - \frac{\nu_m A_3}{v_f A_0 E_m} \tag{28}$$

$$D_{3s} = \frac{1}{2}(\alpha_A - \alpha_m) \tag{29}$$

$$D_3 = D_{3s} - \frac{v_m A_3}{v_f A_0}[\alpha_T - \alpha_m] \tag{30}$$

Here E_A and E_T are the axial and transverse moduli of the fibre, ν_A and ν_T are the axial and transverse Poisson's ratios of the fibre, E_m is the modulus of the matrix, ν_m in the Poisson's ratio of the matrix, α_A and α_T are the axial and transverse thermal expansion coefficients of the fibre, and α_m is the thermal expansion coefficient of the matrix. The fibre is treated as transversely isotropic with the axial direction along the axis of the fibre and the matrix is isotropic. The results for isotropic fibres are easily generated be setting $E_A = E_T = E_f$, $\nu_A = \nu_T = \nu_f$, and $\alpha_A = \alpha_T = \alpha_f$ where subscript f indicates thermomechanical properties of an isotropic fibre.

References

1. **Liu, C. H., and Nairn, J. A.**, "Analytical Fracture Mechanics of the Microbond Test Including the Effects of Friction and Thermal Stresses," *J. of Adhes. and Adhesives.*, **19** (1999), 59–70.
2. **Miller, B., Muri, P., and Rebenfeld, L.**, "A Microbond Method for Determination of the Shear Strength of a Fiber/Resin Interface," *Comp. Sci. & Tech.*, **28** (1987), 17–32.
3. **Penn, L. S., and Bowler, E. R.**, "A New Approach to Surface Energy Characterization for Adhesive Performance Prediction," *Surf. Interf. Anal.*, **3** (1981), 161–164.
4. **Nairn, J. A.**, "On the Use of Shear-Lag Methods for Analysis of Stress Transfer in Unidirectional Composites," *Mech. of Materials*, **26** (1997), 63–80.
5. **Nairn, J. A.**, "Exact and Variational Theorems for Fracture Mechanics of Composites with Residual Stresses, Traction-Loaded Cracks, and Imperfect Interfaces," *Int. J. Fract.*, **in press** (1999).
6. **McCartney, L. N.**, "New Theoretical Model of Stress Transfer Between Fibre and Matrix in a Uniaxially Fibre-Reinforced Composite," *Proc. R. Soc. Lond.*, **A425** (1989), 215–244.
7. **Andrews, M. C., Bannister, D. J., and Young, R. J.**, "Review: The Interfacial Properties of Aramid/Epoxy Model Composites," *J. Mat. Sci.*, **31** (1996), 3893–3913.
8. **Scheer, R. J., and Nairn, J. A.**, "A Comparison of Several Fracture Mechanics Methods for Measuring Interfacial Toughness with Microbond Tests," *J. Adhesion*, **53** (1995), 45–68.
9. **Hashin, Z.**, "Analysis of Properties of Fiber Composites with Anisotropic Constituents," *J. Appl. Mech.*, **46** (1979), 543–549.
10. **Christenson, R. M.**, *Mechanics of Composite Materials*, John Wiley & Sons, New York, 1979.
11. **McCartney, L. N.**, "Analytical Models of Stress Transfer in Unidirectional Composites and Cross-Ply Laminates, and Their Application to the Prediction of Matrix/Transverse Cracking," *Local Mechanics Concepts for Composite Material Systems*, (Eds., J. N. Reddy and K. L Reifsnider), Proc. IUTAM Symposium, Blacksburg, VA (1991), 251–282.
12. **Nayfeh, A. H.**, "Thermomechanically Induced Interfacial Stresses in Fibrous Composites," *Fibre Sci. & Tech.*, **10** (1977), 195–209.
13. **Cox, H. L.**, "The Elasticity and Strength of Paper and Other Fibrous Materials," *Brit. J. Appl. Phys.*, **3** (1952), 72–79.
14. **Zhandarov, S., Pisanova, E., Mäder, E., and Nairn, J. A.**, "Investigation of Load Transfer Between the Fiber and the matrix in Pull-Out Tests with Fibers Having Different Diameters.," *J. Adhesion Sci. & Tech.*, **in press** (2000).
15. **Krishnamurthy, T., Ramamurthy, T. S., Vijayakumar, K. and Dattaguru, B.**, "Modified Crack Closure Integral Method for Higher Order Finite Elements," *Proc. Int. Conf. Finite Elements in Computational Mechanics*, 2-6 December 1985, Bombay, India (1985).
16. **Mertz, S., Auersch, W., Marotzke, C., Schulz, E., and Hampe, A.**, "Investigation of Morphology-Dependent Fracture Behaviour with the Single-Fibre Pull-Out Test," *Comp. Sci. & Tech.*, **48** (1993), 285–290.
17. **Zhandarov, S., Pisanova, E. and Mäder, E.**, "Is There Any Contradiction between the Stress and Energy Failure Criteria in Micromechanical Tests? Pt II. Crack Propagation: Effect of Friction on Force-Displacement Curves," *Composite Interfaces*, **in press** (2000).
18. **Mäder, E., Zhou, X.-F., Pisanova, E., Zhandarov, S., and Nutt, S. R.**, "Characterization of the Interfacial Bond Strength between Glass Fibre and Epoxy Resin Using the Pull-Out and Push-Out Techniques," *Advanced Composites Letters*, **in press** (2000).

19. J. A. Nairn, "Fracture Mechanics Analysis of Single-Fiber Pull-Out and Microbond Tests," `http://www.mse.utah.edu/~nairn/papers/debondFM.html`.